A wearable and sensitive carbon black-porous polydimethylsiloxane based pressure sensor for human physiological signals monitoring

Ningyu Yuan[1], Chenyu Wang[1], Jiuyu Ji[1,*] (ID), and Kun Zhou[1]

[1] School of Information and Control Engineering, Liaoning Petrochemical University, No. 1 Dandong Road West, Fushun 113001, Liaoning, People's Republic of China

ABSTRACT

Development of flexible, low cost, highly sensitive, and large-area compliance pressure sensors that can detect human physiological signals have become one of the vital component units for wearable electronics. Herein, a highly flexible and stretchable carbon black-porous polydimethylsiloxane-based pressure sensor has been successfully fabricated using a simple and effective fabrication technique with a sacrificial power template method. The pore size on the performance of pressure sensor is systematically investigated using KCl, NaCl, and sugar as powder templates to produce the porous PDMS. Notably, the KCl-templated PDMS pressure sensor exhibits a maximum pressure sensitivity (1.07 kPa^{-1} in 0–2 kPa), which is significantly higher than that of the NaCl-templated PDMS pressure sensor (0.86 kPa^{-1} in 0–2.5 kPa) and the sugar-templated PDMS pressure sensor (0.40 kPa^{-1} in 0–2.8 kPa). The KCl-templated PDMS pressure sensor has other advantages as well, including a fast response time of -16 ms, a wide sensing range of 0–11,700 Pa, a low detection limit of -2 mN, and a good reproducibility for over 3000 cycles. With these advantages, it is demonstrated that the pressure sensor can monitor minute mechanical events and human physiological signals, such as weak airflow blown, swallowing motion, finger touch, and pronunciation. Therefore, this new pressure sensor, which exhibit excellent comprehensive performance, will have wide application prospects in health monitoring and wearable devices.

1 Introduction

Flexible pressure sensors are devices that can be mounted on human skin to closely and continuously monitor an individual's motions, without limiting or interrupting the user's activities and thus are very important for extensive potential applications in future, including wearable devices, electronic skins, portable healthcare monitors, and human–machine interfacing [1–4]. Over the past few years, flexible

---

pressure sensors have been extensively concerned by researchers because of their potential advantages, including high sensitivity, mechanical flexibility, fast response time, simple fabrication process, and low cost [5–10]. To date, four main sensing mechanisms, including piezocapacitive [11, 12], piezoresistive [13–15], piezoelectric [16], and triboelectric effects [17, 18], have been adopted to fabricate flexible pressure sensors. Among these types of sensors, piezoresistive pressure sensors, which transduce pressure into a resistance signal, have been widely explored because of their high sensitivity, easy signal collection, low energy consumption, and simple device assembly [19].

Combining conductive materials with other elastomeric materials is one of the typical ways to obtain high-performance piezoresistive pressure sensors. Up to now, this type of piezoresistive pressure sensors have been prepared using sensing fillers including conductive materials (reduced graphene oxide (rGO) [20], graphene [21], carbon nanotubes (CNT) [3, 22], Ag nanowires [23], and Au nanowires [24]); these conductive filling materials are typically embedded in elastomeric materials (polydimethylsiloxane (PDMS) [8, 25–30] and Ecoflex [31, 32]). It is revealed that electrical current is transported through the network of conductive nanomaterials in these composites. When a pressure is applied, the distance between conductive nanomaterials is reduced and electrical current can be transported more easily. However, manufacturing process of elastomer-based conductive nanocomposites is relatively complex and multi-step, since in general a homodisperse of conductive fillers is achieved only through chemical modification with functional groups. Furthermore, a relatively high loading is usually required to achieve the target electrical conductivity, although it leads to a severe degradation of the initial mechanical properties [33, 34].

Recently, flexible piezoresistive pressure sensors utilizing three-dimensional (3D) polymer foams coated with conductive nanomaterials have drawn considerable attention [35–38] due to excellent elastic characteristics of porous polymers, which obviously exceeds that of their solid counterparts [39], as well as superior dispersion properties of conductive nanomaterials in the porous polymer, which greatly improves electrical conductivity of the nanocomposites [40]. For instance, Song et al. reported flexible PDMS sponges coated with CNTs, which is fabricated by drop-casting solution into sacrificial sugar cubes. The sensor can detect pressure and strain in the range 26 Pa–150 kPa and 10–60%, respectively [41]. Yao et al. realized a pressure sensor exploiting graphene-wrapped polyurethane (PU) sponges coated with graphene oxide nanosheets using drop-casting method, which can reliably monitor a minimum pressure of 9 Pa, up to 2 kPa [42]. However, the polymer foams are fragile, which lead to a poor stability of the devices over extended cyclic testing [38, 43]. Moreover, to achieve measurable changes in conductivity upon deformation, thick foams need to be considered. However, thick foams are bulky on the surface of the skin [44, 45]. Therefore, simple template methods to fabricate thin porous films have been developed [46–48]. Over the past few years, various compressible and flexible PDMS sponges have been fabricated by the sacrificial power template (e.g., KCl, NaCl, and sugar) method. Flexible conductive sponge can also be fabricated using the sacrificial power template method by incorporating conductive nanomaterials during sponge preparation or by drop-casting conductive solution after sponge preparation. The flexible pressure sensors based on silver nanowire/porous PDMS (pPDMS) [49] and multi-walled CNTs/pPDMS [44] through template method have been previously reported, which present an improved performance. The conductive nanomaterials used in aforementioned pressure sensors have achieved good performances and attracted a great amount of scientific attention. However, most of metal nanomaterials are susceptible to oxidization in ambient environment and noble metal nanowires are stable but costly. Some carbon nanomaterials, such as CNTs and graphene, are costly and complicated to be prepared during the fabrication processes, which limit their widespread practical applications in the future. On the contrary, CB has excellent chemical stability in ambient environment and could be mass produced at low cost.

In this work, we design a low cost and simple approach for the fabrication of flexible and highly sensitive piezoresistive pressure sensor based on CB and pPDMS. The pPDMS is synthesized using different powders as sacrificial templates. CB is uniformly coated onto pPDMS using the drop-casting method to construct CB/pPDMS composites. The pore size on the performance of pressure sensor is systematically investigated by utilizing KCl, NaCl,

and sugar as sacrificial templates to produce the pPDMS layers, respectively. The pressure sensor is applied to detect minute mechanical events and human physiological signals, including weak airflow blown, swallowing motion, finger touch, and pronunciation. Therefore, this new pressure sensor, which exhibits excellent comprehensive performance, will have wide application prospects in health monitoring and wearable devices.

2 Experimental section

2.1 Chemicals and reagents

Commercially available sugar, polyimide tapes, and copper tapes were used as received. PDMS Sylgard 184 base (component *A*) and thermal curing agent (component B) were achieved from Sigma-Aldrich. Conductive CB was purchased from XFNANO Materials Tech Co., Ltd., China. The other solvents and reagents, including ethanol, acetone, KCl, and NaCl, were used without further purification.

2.2 Synthesis of pPDMS

The PDMS precursor (*A*:*B* = 10:1) was degassed in a vacuum chamber for 3 min to remove the trapped bubbles. Subsequently, a liquid PDMS layer was formed by pouring PDMS precursor onto a glass substrate with automatic leveling process. Then KCl, NaCl, and sugar powders were spread on the liquid PDMS layer by utilizing a 100-mesh sieve. After being kept at 80 °C for 2 h in the oven, the powders were embedded in the cured PDMS layer. The embedded powders were removed by soaking into deionized water for about 40 min, resulting in a thin pPDMS layer.

2.3 Synthesis of CB/pPDMS composites

The CB/pPDMS composites were obtained by drop-casting CB-DMF solution into pPDMS. In detail, 0.2 g of CB was added into 100 mL of DMF to prepare the CB solution, in which the diameter of CB nanoparticles was − 30 nm. To improve the dispersity of the CB suspension, the resulting solution was sonicated for 30 min. Then, 0.8 mL of CB solution was dropped into the pPDMS by pipette. Next, the CB/pPDMS was dried at 110 °C on a heating plate. Meanwhile,

CB was left inside the pores and forms a thin conducting coating adhering through interfacial forces. Finally, the resistance of the CB/pPDMS composite can be adjusted by the concentration of CB solution.

2.4 Fabrication of the flexible CB/pPDMS pressure sensors

The CB/pPDMS composites were sandwiched between the copper tapes as electrodes. Then, the pPDMS-based pressure sensor was packaged by polyimide tapes, thus producing the CB/pPDMS pressure sensor with outstanding compatibility and flexibility.

2.5 Characterization

The morphology and chemical composition of samples were observed using a XL30 ESEM FEG scanning electron microscope (SEM) at an accelerating voltage of 20 kV. The piezoresistive performances of the CB/pPDMS composite were collected by an electrochemical workstation (CHI 760E, ChenHua). The cyclic stability of the sensor was measured under 2.5 kPa pressure applied by a shaker vibrator at a frequency of 1 Hz. The current response is defined by the ratio of the change in current (ΔI) and the original-based current (I_0).

# 3 Results and discussion

3.1 Preparation of the CB/pPDMS composites

The fabrication procedure and overall design concept are described as follows. First of all, the pPDMS is fabricated via a sacrificial power template method using KCl, NaCl, and sugar powder as sacrificial template. The excessive sacrificial powder is spread on the flat of the PDMS prepolymer layer by sieving process. Then, a glass plate is placed on the top of the surface and two clamps are used to apply a pressure onto the PDMS prepolymer during the curing process. In this case, the sacrificial powder realizes a dense accumulation and uniformly distributes throughout the PDMS prepolymer layer. At last, the CB/pPDMS composites are fabricated by drop-casting CB dispersions onto pPDMS. The resistance of the CB/pPDMS composites can be adjusted by the

concentration of CB solution. To optimize the electrical conductivity of CB/pPDMS composites, a systematic study has been investigated about the relationship between the CB solution concentration and the sheet resistance, as shown in Fig. 1. The results exhibit that the average sheet resistance decreases from 350 kΩ to 0.5 kΩ (1×1 cm^2) with the concentration of CB solution increasing from 1.0 to 3.0 mg/mL. In order to optimize device performance, the sheet resistance should be carefully selected. On the one hand, if the sheet resistance is too low, the energy consumption of the pressure sensor will increase, resulting in thermal effect and long-term performance degradation. On the other hand, the resistance values of CB/pPDMS composites prepared with low CB solution concentration have large variation, resulting in low reproducibility of pressure sensors. Thus, 2.0 mg/mL CB solution is selected to fabricate the CB/pPDMS composites with an average resistance of 45 kΩ (1×1 cm^2).

After templating, the resulting pPDMS films are porous and thin but not greatly fragile. The films are obviously shinier on one side than the other, indicating that one surface is made up by a thin continuous layer of PDMS. The morphologies of pPDMS template from different sacrificial powder and pPDMS template after coating with CB are characterized by SEM. Figure 2a, d, and g shows the pPDMS template from KCl, NaCl, and sugar, respectively, while Fig. 2b, e, and h shows the corresponding pPDMS template after coating with CB, respectively. The structure of the sacrificial powder is
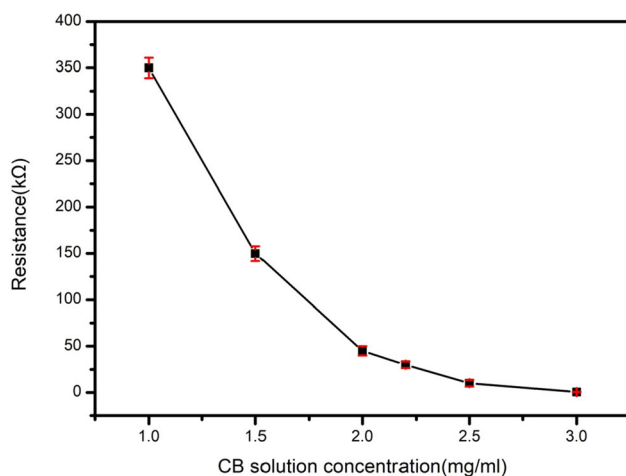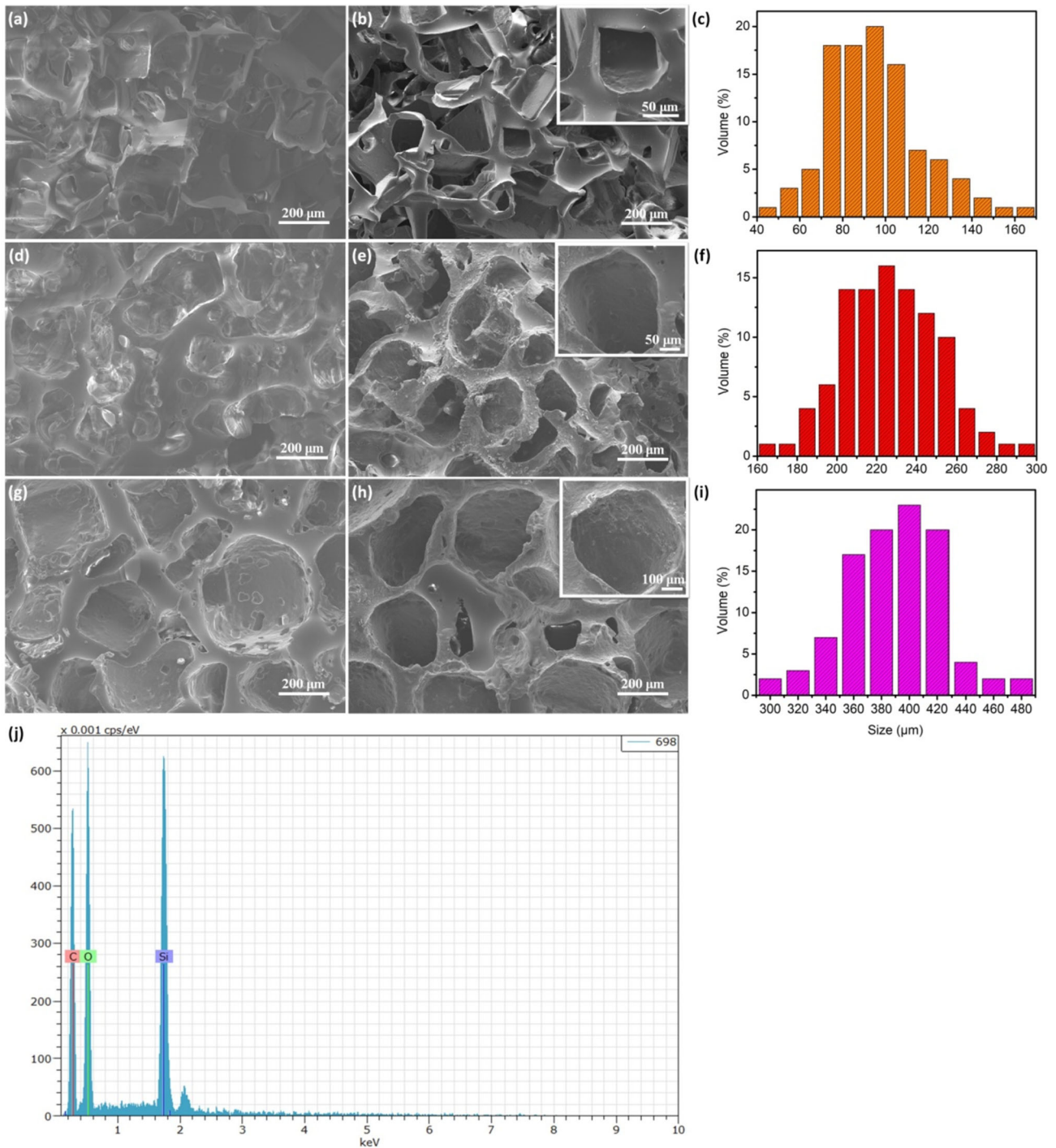
perfectly replicated in the pPDMS template. For different sacrificial powders, pores with an approximately cubic shape are uniformly distributed on the surface of PDMS and the diameter of the pores is comparable size to the sacrificial powders. Some smaller pores are observed in the pPDMS template, which is due to the uneven size of the sacrificial powders. To quantify the pore size distribution, the Nano Measurer software is used, and the results for KCl, NaCl, and sugar templates are shown in Fig. 2c, f, and i, respectively. From the bar chart, it can be seen that the size of the pores produced by KCl range from 70 to 110 μm, while those produced by NaCl and sugar range from 200 to 260 μm and 350 to 430 μm, respectively. The average size of the pores produced by KCl, NaCl, and sugar templates are about 97 μm, 227 μm, and 389 μm, respectively. It is obvious that the size of the pores produced by KCl is the smallest, while the size of the pores produced by sugar is the largest.

As shown in Fig. 2b, e, and h, after coating the pPDMS with a layer of CB nanoparticles, the CB/pPDMS composites exhibit a rough surface structure, indicating that the CB is uniformly coated onto the surface of pPDMS. The pores are conformally coated by the drop-casting method and therefore remain open in exterior structure and have same size and shape to the pores in the uncoated samples. EDX spectrum of the pPDMS template after coating with CB is shown in Fig. 2j. It displays C, O, and Si peaks, which reveal that CB are indeed decorated on the surface of pPDMS template. Note that the existence of O and Si signals result from the pPDMS template.

3.2 Pressure sensing performance of the CB/pPDMS pressure sensor

To systematically evaluate the sensing performance of the prepared CB/pPDMS composites, a series of compression tests are performed on the KCl-templated PDMS sensors. The CB/pPDMS composites are sandwiched between the copper tapes as electrodes. The piezoresistive structure and electrodes are packaged by polyimide tapes. This simple encapsulation not only prevents direct contact between human skin and CB but also enables the CB/pPDMS composite to be firmly bonded to the electrode to improve the mechanical strength of the sensor. Figure 3a shows the I–V curves of KCl-templated PDMS pressure sensor under a wide range of

Fig. 1 The relationship between the sheet resistance of 1 cm × 1 cm CB/pPDMS composite and the concentration of CB solution

Fig. 2 **a**, **d**, **g** SEM images of pPDMS template from KCl, NaCl, and sugar, respectively. **b**, **e**, **h** SEM images of pPDMS template after coating with CB from KCl, NaCl, and sugar, respectively. Insets are the corresponding high-magnification images. **c**, **f**, **i** Pore distribution charts of each sample (shown in the same order as previously) depicting the percent of pores of each size range in the images surveyed. **j** EDX spectrum of the pPDMS template after coating with CB

applied pressures, which exhibits a linear behavior, indicating the formation of ohmic contacts between CB/pPDMS composites and conductive electrodes.

The slope of the I–V curves increases as the applied pressures increases, indicating the resistance decrease when an external pressure is applied on the

sensor. The pressure sensor is applied under different pressures to test its sensitivity to applied pressures. As shown in Fig. 3b, the KCl-templated PDMS pressure sensor is applied with cyclic loading–unloading tests under the various pressure values of 35, 120, 240, 1200, 2500, and 8500 Pa. The results show that the $\Delta I/I_0$ values increase regularly with the increase of applied pressures and the sensor has a wide sensing range, suggesting that the sensor not only monitors a small pressure but also monitors a large pressure. The pressure responsive property of the KCl-templated PDMS pressure sensor is investigated. Figure 3c presents the current response against the applied pressure curve of the sensor. The calculation of sensitivity (S) is based on the formula $S = \delta\,(\Delta I/I_0)/\delta P$. Similar to most reported pressure sensors [50], the plot for sensitivity is consisted of multiple regions. In the range of 35–2000 Pa, the current variation ΔI almost linearly increases with the pressure variation (δP) and the sensitivity S_1 is 1.07 kPa^{-1}. In the range of 2000–11,700 Pa, the sensitivity S_2 decreases to 0.10 kPa^{-1} with the further increase of pressure. Figure 3d presents the current response of the pressure sensor under cyclic loading–unloading tests with different frequencies under a pressure of about

3.0 kPa. The response signal of the sensor is highly stable and independent of the loading rate, which is of great significance to the practical applications of the sensor. The response/recovery time is also a significant parameter for evaluating the sensing performances. As presented in Fig. 3e, the response time and recovery time of the KCl-templated PDMS pressure sensor are − 50 and − 16 ms, when the applied pressure is 2.5 kPa. It indicates that the KCl-templated PDMS pressure sensor has a high sensitivity and short response time. The reliability test of the sensor is shown in Fig. 3f. Under a pressure of about 2.5 kPa and a frequency of 1 Hz, 3000 cycle tests were carried out with the loading/unloading pressure. From the signal figure, it is revealed that the KCl-templated PDMS pressure sensor has good reproducibility, displaying that the air gaps can still exist stably under repeated pressure.

In order to study the influence of the size of the pores on the sensing performance, a series of experiments are carried out. The current response as a function of applied pressure for pressure sensor template from KCl, NaCl, and sugar powder is shown in Fig. 4a. For all devices, the resistance generally decreases as pressure is applied, which is due
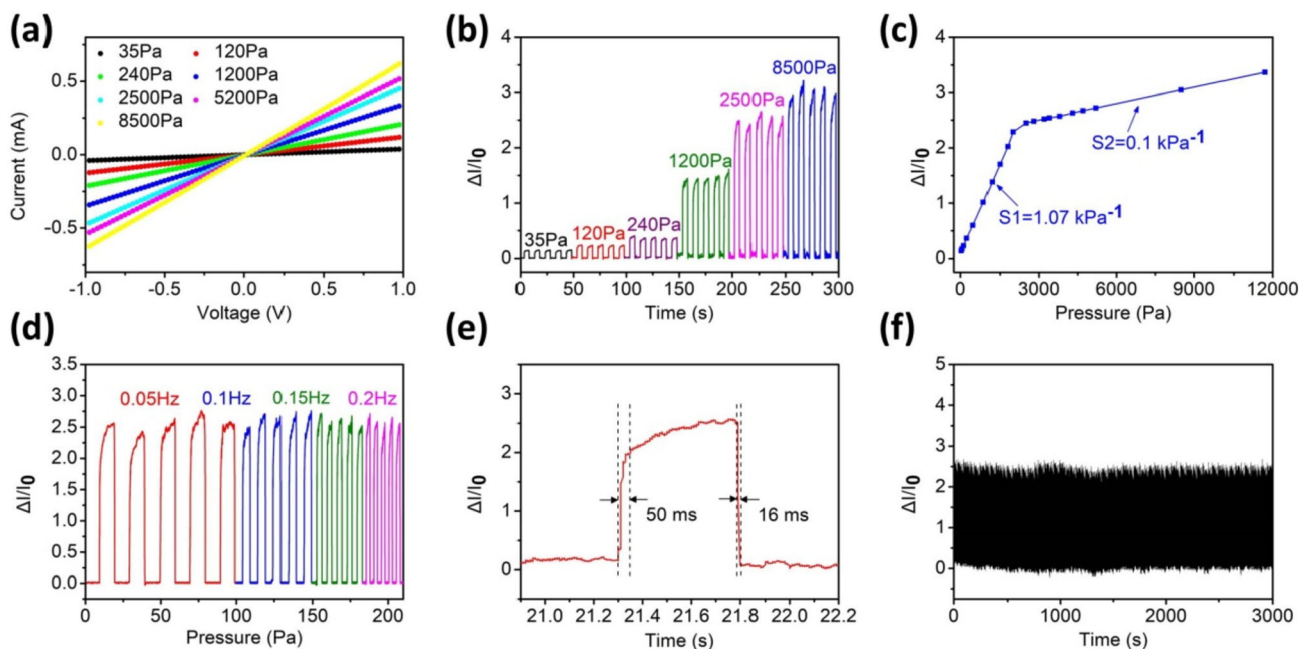
Fig. 3 The basic electromechanical performance of the KCl-templated PDMS pressure sensors. **a** Corresponding *I–V* curves under various pressures. **b** The current response under various applied pressures ranging from 35 to 8500 Pa. **c** The current response against the applied pressure. **d** The current response of the pressure sensor under cyclic loading and unloading at different frequencies. **e** The responsive time and recovery time of the pressure sensor. **f** Stability performance of the pressure sensor under more than 3000 loading and unloading cycles

to that the contact area between the CB on the surface of each porous layer is increased under pressure. Thus, it is obvious that an increase in current response occurs for all samples as the pressure increased. With the increase of pressure, the variation of the current response begins to be large (rapidly increasing) and then decreases at higher pressures (i.e., the slope becomes smaller), indicating that the deformation at higher pressures is more limited. For devices templated from the smallest powders (i.e., KCl and NaCl), the overall response is larger and more consistent. The sensitivity of the pressure sensor is calculated by taking the slope of the initial linear part of the curve. The sensitivity for device templated from KCl is 1.07 kPa^{-1} in 0–2 kPa; the sensitivity for device templated from NaCl is 0.86 kPa^{-1} in 0–2.5 kPa; the sensitivity for device templated from sugar is 0.40 kPa^{-1} in 0–2.8 kPa. The device templated from KCl has the highest sensitivity, which is due to its smaller porous and larger surface area-to-volume ratio compared to other device. Then, when a pressure is applied, the devices with smaller porous can increase relatively more contact area between the CB on the surface of each porous layer and the conductivity increases accordingly.

The response and recovery times of these pressure sensors are shown in Fig. 4b. It can be seen that the responses of the three devices have no obvious time delay upon unloading, but all the devices have time delay upon initial loading. Specifically, the pressure sensor made with KCl-templated PDMS has the

fastest recovery time − 16 ms, while pressure sensor made with sugar-templated PDMS has the slowest recovery time − 37 ms. Compared to the other two types of devices, pressure sensor made with NaCl-templated PDMS has moderately sized pores with a recovery time of − 26 ms. The hysteresis of the pressure sensors is mainly caused by the stiffness of the porous layers and the stiffness of the porous layer is affected by the size of the pores. The KCl-templated PDMS layers are the stiffest, while sugar-templated PDMS samples are the softest.
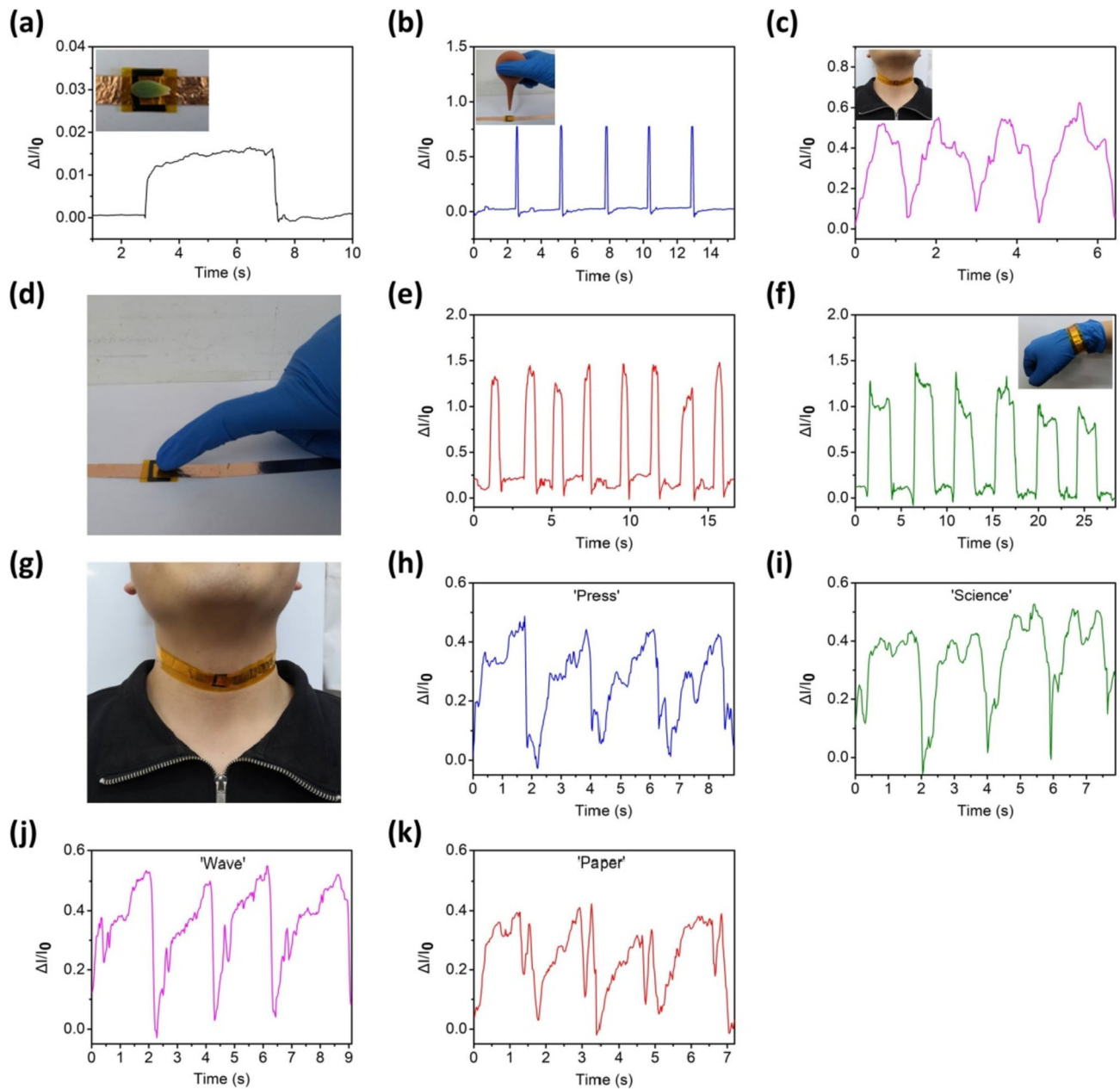
3.3 Applications of the flexible CB/pPDMS pressure sensor

The KCl-templated PDMS pressure sensor is a good candidate for detecting minute mechanical events and physiological signals due to its high sensitivity and broad pressure measurement range. Figure 5a presents the current response that a small leaf of succulent plant is loaded/removed onto the KCl-templated PDMS pressure sensor, which suggests our pressure sensor can detect tiny pressure below − 2 mN. In addition, the sensor can also detect the weak airflow blown by rubber suction bulb, which benefits from low detection limit and high sensitivity of the KCl-templated PDMS pressure sensor. The testing curve of the pressure sensor is shown in Fig. 5b. Figure 5c shows the KCl-templated PDMS pressure sensor attached to human neck by polyimide tapes. The pressure sensor can effectively detect the swallowing motion when the tester imitates swallowing. Afterward, we tap repeatedly the
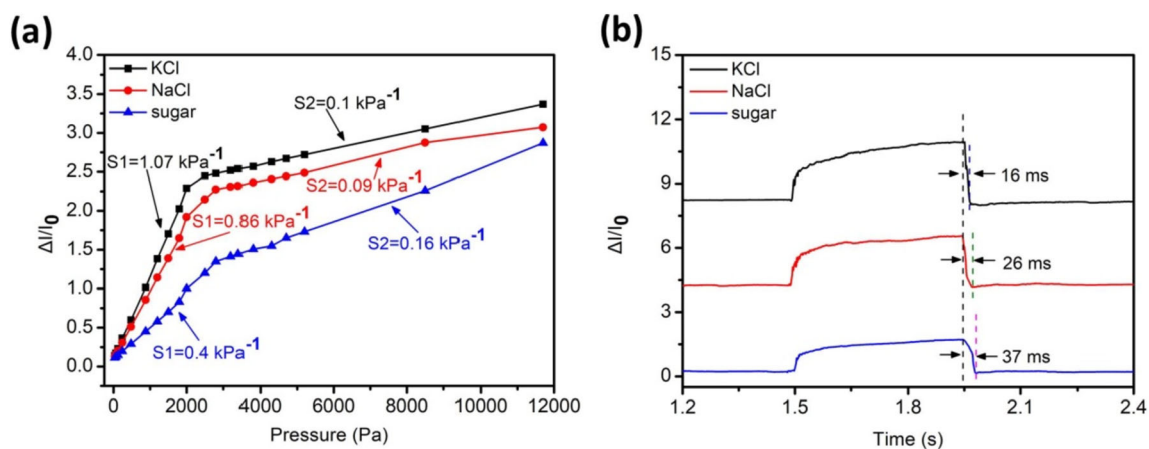
Fig. 4 Characterization of devices fabricated using NaCl-templated PDMS, KCl-templated PDMS, and sugar-templated PDMS: **a** The current response as a function of applied pressure, **b** the responsive time and recovery time of devices upon loading and unloading of 3 kPa pressure

Fig. 5 Applications of the KCl-templated PDMS pressure sensor for various minute mechanical events and physiological signals' monitoring in real time. **a** The current response of the pressure sensor when loading/removing a small leaf of succulent plant. **b** The current response of the pressure sensor blown by a rubber suction bulb. **c** The current response of the pressure sensor mounted on the neck for tracking the swallowing motion. **d** Photograph showing the pressure sensor pressed by a finger and **e** the corresponding current response. **f** The current response of the pressure sensor fixed on the back of the wrist for tracking wrist bending. **g** Photograph showing a pressure sensor pasted on a human neck for voice recognition and the response curves induced by phonation of **h** "Press," **i** "Science," **j** "Wave," and **k** "Paper," respectively

pressure sensor with finger (Fig. 5d), the curve of current response exhibits sharp peak in Fig. 5e, which is due to the pressure of the finger. In addition, the pressure sensor attached to the back of the wrist joint can identify bending deformation in Fig. 5f,

which provides a promising approach in monitoring the exercise state of athletes during training. It is observed that the current response of the pressure sensor increased significantly when the wrist was bended. The pronunciation signals can be detected by

this pressure sensor attached to the throat, because the muscular movements of pronunciation will produce a special force. Figure 5g shows the pressure sensor mounted onto human neck by polyimide tapes. The response signals of the pressure sensor show significantly different patterns when pronouncing the words "Press," "Science," "Wave," and "Paper" and the signal curves for each word have identical characteristic peaks (Fig. 5h–k). This monitoring of pronunciation could lead to the development of artificial intelligence for identity distinguishing.

4 Conclusion

In this work, we design a low cost and simple templating method for the fabrication of flexible and high sensitivity piezoresistive pressure sensor based on CB and pPDMS. The pore size on the performance of pressure sensor is systematically investigated by utilizing KCl, NaCl, and sugar as sacrificial templates to produce the pPDMS layers. It is demonstrated that the sensors fabricated with KCl porous layers exhibit the best performance, with a sensitivity of 1.07 kPa^{-1} in 0–2 kPa, a fast response time of $-$ 16 ms, and a good stability over 3000 cycles. In addition, the pressure sensor can monitor minute mechanical events and human physiological signals, such as weak airflow blown, swallowing motion, finger touch, and pronunciation. We believe that this pressure sensor with low cost, ultralow energy consumption, and high sensitivity will have great potential in flexible electronic devices in the future.

Acknowledgements

References

1. C.M. Boutry, L. Beker, Y. Kaizawa, C. Vassos, H. Tran, A.C. Hinckley, R. Pfattner, S. Niu, J. Li, J. Claverie, Z. Wang, J. Chang, P.M. Fox, Z. Bao, Nat. Biomed. Eng. **3**, 47 (2019)

2. S. Lee, D. Sasaki, D. Kim, M. Mori, T. Yokota, H. Lee, S. Park, K. Fukuda, M. Sekino, K. Matsuura, T. Shimizu, T. Someya, Nat. Nanotechnol. **14**, 156 (2019)

3. K. Takei, T. Takahashi, J.C. Ho, H. Ko, A.G. Gillies, P.W. Leu, R.S. Fearing, A. Javey, Nat. Mater. **9**, 821 (2010)

4. Y.J. Hong, H. Jeong, K.W. Cho, N. Lu, D.H. Kim, Adv. Funct. Mater. **29**, 1808247 (2019)

5. C. Yang, L. Li, J. Zhao, J. Wang, J. Xie, Y. Cao, M. Xue, C. Lu, A.C.S. Appl, Mater. Interfaces **10**, 25811 (2018)

6. S.M. Doshi, E.T. Thostenson, ACS Sens. **3**, 1276 (2018)

7. Y. Li, Y.A. Samad, T. Taha, G. Cai, S.-Y. Fu, K. Liao, ACS Sustain. Chem. Eng. **4**, 4288 (2016)

8. C. Yan, J. Wang, W. Kang, M. Cui, X. Wang, C.Y. Foo, K.J. Chee, P.S. Lee, Adv. Mater. **26**, 2022 (2014)

9. L.Q. Tao, K.N. Zhang, H. Tian, Y. Liu, D.Y. Wang, Y.Q. Chen, Y. Yang, T.L. Ren, ACS Nano **11**, 8790 (2017)

10. M. Han, H. Wang, Y. Yang, C. Liang, W. Bai, Z. Yan, H. Li, Y. Xue, X. Wang, B. Akar, H. Zhao, H. Luan, J. Lim, I. Kandela, G.A. Ameer, Y. Zhang, Y. Huang, J.A. Rogers, Nat. Electron. **2**, 26 (2019)

11. R. Nur, N. Matsuhisa, Z. Jiang, M.O.G. Nayeem, T. Yokota, T. Someya, Nano Lett. **18**, 5610 (2018)

12. Y. Wan, Z. Qiu, J. Huang, J. Yang, Q. Wang, P. Lu, J. Yang, J. Zhang, S. Huang, Z. Wu, C.F. Guo, Small **14**, 1801657 (2018)

13. Z. Han, Z. Cheng, Y. Chen, B. Li, Z. Liang, H. Li, Y. Ma, X. Feng, Nanoscale **11**, 5942 (2019)

14. A. Tewari, S. Gandla, S. Bohm, C.R. McNeill, D. Gupta, A.C.S. Appl, Mater. Interfaces **10**, 5185 (2018)

15. S. Wagner, C. Yim, N. McEvoy, S. Kataria, V. Yokaribas, A. Kuc, S. Pindl, C.-P. Fritzen, T. Heine, G.S. Duesberg, M.C. Lemme, Nano Lett. **18**, 3738 (2018)

16. E.J. Curry, K. Ke, M.T. Chorsi, K.S. Wrobel, A.N. Miller, A. Patel, I. Kim, J. Feng, L. Yue, Q. Wu, C.-L. Kuo, K.W.-H. Lo, C.T. Laurencin, H. Ilies, P.K. Purohit, T.D. Nguyen, Proc. Natl. Acad. Sci. USA **115**, 909 (2018)

17. J. Zou, M. Zhang, J. Huang, J. Bian, Y. Jie, M. Willander, X. Cao, N. Wang, Z.L. Wang, Adv. Energy Mater. **8**, 1702671 (2018)

18. Y.-C. Lai, J. Deng, R. Liu, Y.-C. Hsiao, S.L. Zhang, W. Peng, H.-M. Wu, X. Wang, Z.L. Wang, Adv. Mater. **30**, 1801114 (2018)

19. M. Jian, K. Xia, Q. Wang, Z. Yin, H. Wang, C. Wang, H. Xie, M. Zhang, Y. Zhang, Adv. Funct. Mater. **27**, 1606066 (2017)

20. B. Zhu, Z. Niu, H. Wang, W.R. Leow, H. Wang, Y. Li, L. Zheng, J. Wei, F. Huo, X. Chen, Small **10**, 3625 (2014)

21. Y. Ma, L. Zhi, Small Methods **3**, 1800199 (2019)

22. C. Stampfer, T. Helbling, D. Obergfell, B. Schoberle, M.K. Tripp, A. Jungen, S. Roth, V.M. Bright, C. Hierold, Nano Lett. **6**, 233 (2006)

23. H.-J. Kim, A. Thukral, C. Yu, A.C.S. Appl, Mater. Interfaces **10**, 5000 (2018)

24. S. Gong, W. Schwalb, Y. Wang, Y. Chen, Y. Tang, J. Si, B. Shirinzadeh, W. Cheng, Nat. Commun. **5**, 3132 (2014)

25. J.H. Kong, N.S. Jang, S.H. Kim, J.M. Kim, Carbon **77**, 199 (2014)

26. T. Yamada, Y. Hayamizu, Y. Yamamoto, Y. Yomogida, A. Izadi-Najafabadi, D.N. Futaba, K. Hata, Nat. Nanotechnol. **6**, 296 (2011)

27. J. Zhou, H. Yu, X. Xu, F. Han, G. Lubineau, A.C.S. Appl, Mater. Interfaces **9**, 4835 (2017)

28. J.R. Jeong, H. Park, S.W. Jin, S.Y. Hong, S.S. Lee, J.S. Ha, Adv. Funct. Mater. **25**, 4228 (2015)

29. S. Chen, Z. Lou, D. Chen, K. Jiang, G. Shen, Adv. Mater. Technol. **1**, 1600136 (2016)

30. J. Lee, S. Kim, J. Lee, D. Yang, B.C. Park, S. Ryu, I. Park, Nanoscale **20**, 1 (2014)

31. S. Ryu, P. Lee, J.B. Chou, R. Xu, R. Zhao, A.J. Hart, S.G. Kim, ACS Nano **9**, 5929 (2015)

32. J.T. Muth, D.M. Vogt, R.L. Truby, Y. Mengüç, D.B. Kolesky, R.J. Wood, J.A. Lewis, Adv. Mater. **26**, 6307 (2014)

33. N. Luo, W. Dai, C. Li, Z. Zhou, L. Lu, C.C.Y. Poon, S.-C. Chen, Y. Zhang, N. Zhao, Adv. Funct. Mater. **26**, 1178 (2016)

34. Y. Ma, Y. Yue, H. Zhang, F. Cheng, W. Zhao, J. Rao, S. Luo, J. Wang, X. Jiang, Z. Liu, N. Liu, Y. Gao, ACS Nano **12**, 3209 (2018)

35. H. Zhang, N. Liu, Y. Shi, Y. Yue, S. Wang, Y. Ma, L. Wen, L. Li, F. Long, Z. Zou, Y. Gao, A.C.S. Appl, Mater. Interfaces **8**, 22374 (2016)

36. H. Chen, Z. Su, Y. Song, X. Cheng, X. Chen, B. Meng, Z. Song, D. Chen, H. Zhang, Adv. Funct. Mater. **27**, 1604434 (2016)

37. J. Li, S. Zhao, X. Zeng, W. Huang, Z. Gong, G. Zhang, R. Sun, C.P. Wong, A.C.S. Appl, Mater. Interfaces **8**, 18954 (2016)

38. L. Lv, P. Zhang, T. Xu, L. Qu, A.C.S. Appl, Mater. Interfaces **9**, 22885 (2017)

39. J. Park, S. Wang, M. Li, C. Ahn, J.K. Hyun, D.S. Kim, D.K. Kim, J.A. Rogers, Y. Huang, S. Jeon, Nat. Commun. **916**, 1 (2012)

40. M. Chen, L. Zhang, S. Duan, S. Jing, H. Jiang, C. Li, Adv. Funct. Mater. **24**, 7548 (2014)

41. Y. Song, H. Chen, Z. Su, X. Chen, L. Miao, J. Zhang, X. Cheng, H. Zhang, Small **13**, 1702091 (2017)

42. H.B. Yao, J. Ge, C.F. Wang, X. Wang, W. Hu, Z.J. Zheng, Y. Ni, S.H. Yu, Adv. Mater. **25**, 6692 (2013)

43. H. Park, J.W. Kim, S.Y. Hong, G. Lee, D.S. Kim, J.H. Oh, S.W. Jin, Y.R. Jeong, S.Y. Oh, J.Y. Yun, J.S. Ha, Adv. Funct. Mater. **28**, 1707013 (2018)

44. R. Iglio, S. Mariani, V. Robbiano, L. Strambini, G. Barillaro, A.C.S. Appl, Mater. Interfaces **10**, 13877 (2018)

45. T. Wang, J. Li, Y. Zhang, F. Liu, B. Zhang, Y. Wang, R. Jiang, G. Zhang, R. Sun, C.-P. Wong, Chem. Eur. J. **25**, 6378 (2019)

46. L. Ding, S. Xuan, L. Pei, S. Wang, T. Hu, S. Zhang, X. Gong, A.C.S. Appl, Mater. Interfaces **10**, 30774 (2018)

47. Y. Gao, G. Yu, J. Tan, F. Xuan, Sens. Actuat. A **280**, 205 (2018)

48. G. Yu, J. Hu, J. Tan, Y. Gao, Y. Lu, F. Xuan, Nanotechnology **29**, 115502 (2018)

49. L. Dan, S. Shi, H.-J. Chung, A. Elias, A.C.S. Appl, Nano Mater. **2**, 4869 (2019)

50. C. Mu, Y. Song, W. Huang, A. Ran, R. Sun, W. Xie, H. Zhang, Adv. Funct. Mater. **28**, 1707503 (2018)